UC San Diego
UC San Diego Previously Published Works

Title

Fecal transplantation and butyrate improve neuropathic pain, modify immune cell profile, and gene expression in the PNS of obese mice

Permalink

https://escholarship.org/uc/item/0bp9g0bp

Journal

Proceedings of the National Academy of Sciences of the United States of America, 117(42)

ISSN

0027-8424

Authors

Bonomo, Raiza R
Cook, Tyler M
Gavini, Chaitanya K
et al.

Publication Date

2020-10-20

DOI

10.1073/pnas.2006065117

Peer reviewed

Fecal transplantation and butyrate improve neuropathic pain, modify immune cell profile, and gene expression in the PNS of obese mice

Raiza R. Bonomo[a] , Tyler M. Cook[a], Chaitanya K. Gavini[a] , Chelsea R. White[a], Jacob R. Jones[b], Elisa Bovo[a] , Aleksey V. Zima[a] , Isabelle A. Brown[a], Lara R. Dugas[c,d] , Eleonora Zakharian[b] , Gregory Aubert[a,e] , Francis Alonzo III[f] , Nigel A. Calcutt[g] , and Virginie Mansuy-Aubert[a,1]

[a]Department of Cell and Molecular Physiology, Stritch School of Medicine, Loyola University Chicago, Maywood, IL 60153; [b]Department of Cancer Biology and Pharmacology, University of Illinois College of Medicine, Peoria, IL 61605; [c]Department of Public Health Sciences, Stritch School of Medicine, Loyola University Chicago, Maywood, IL 60153; [d]Department of Human Biology, University of Cape Town, Cape Town 7935, South Africa; [e]Department of Internal Medicine, Division of Cardiology, Stritch School of Medicine, Loyola University Chicago, Maywood, IL 60153; [f]Department of Microbiology and Immunology, Stritch School of Medicine, Loyola University Chicago, Maywood, IL 60153; and [g]Department of Pathology, University of California San Diego, La Jolla, CA 92093

Obesity affects over 2 billion people worldwide and is accompanied by peripheral neuropathy (PN) and an associated poorer quality of life. Despite high prevalence, the molecular mechanisms underlying the painful manifestations of PN are poorly understood, and therapies are restricted to use of painkillers or other drugs that do not address the underlying disease. Studies have demonstrated that the gut microbiome is linked to metabolic health and its alteration is associated with many diseases, including obesity. Pathologic changes to the gut microbiome have recently been linked to somatosensory pain, but any relationships between gut microbiome and PN in obesity have yet to be explored. Our data show that mice fed a Western diet developed indices of PN that were attenuated by concurrent fecal microbiome transplantation (FMT). In addition, we observed changes in expression of genes involved in lipid metabolism and calcium handling in cells of the peripheral nerve system (PNS). FMT also induced changes in the immune cell populations of the PNS. There was a correlation between an increase in the circulating short-chain fatty acid butyrate and pain improvement following FMT. Additionally, butyrate modulated gene expression and immune cells in the PNS. Circulating butyrate was also negatively correlated with distal pain in 29 participants with varied body mass index. Our data suggest that the metabolite butyrate, secreted by the gut microbiome, underlies some of the effects of FMT. Targeting the gut microbiome, butyrate, and its consequences may represent novel viable approaches to prevent or relieve obesity-associated neuropathies.

obesity | neuropathy | microbiome

Almost half of the United States population is overweight or obese (1). A report from the Institute of Medicine identified obesity as one of five major contributors to chronic pain (2). Obesity raises risks of numerous conditions associated with neuropathic pain, including the use of addictive drugs. Early clinical manifestations of painful peripheral neuropathy are understudied in obese and prediabetic patients, but there is evidence of distal hypersensitivity and pain in the hands and feet (3–6). Despite being one of the most common complications of obesity, treatment of painful neuropathy is frequently limited to use of addictive analgesics, mostly because the neurobiology underlying the complex pain etiology in obesity and prediabetes is poorly understood. In rodent models, hypersensitivity, presenting as mechanical allodynia, is seen as early as 6 to 16 wk after the onset of feeding a Western diet (WD: 42% fat, 34% sucrose, and 0.2% cholesterol) and is followed by loss of epidermal sensory fibers (7–12). It has been shown that neuropathic pain that develops early in a rodent model of prediabetes involves hyperexcitability of

nociceptors (13). Many previous studies have focused on hyperglycemia as the initiating insult in the development of prediabetic and diabetic neuropathy, while a growing body of evidence has also implicated dyslipidemia as a distinct pathogenic event (14–17).

The relationship between the gut microbiota and neurological diseases, including pain, has received increasing attention in recent years. The gut microbiome and its lipid metabolites have been linked to peripheral immune regulation (18–25), visceral pain (26–29), chemotherapy-induced pain (30), and fibromyalgia (31). A recent case report described amelioration of painful neuropathy following fecal microbiome transplantation (FMT) to an obese type 2 diabetic patient (32). We have therefore begun to investigate the role of the gut microbiome in obesity-related neuropathic pain. Our data demonstrate that reshaping the gut microbiome of obese neuropathic mice by transplanting feces from lean mice improved the pathophysiology of the disease by decreasing evoked pain-associated behaviors and loss of nerve fibers in the skin. Sequencing and flow cytometry identified modulation of peripheral nerve system (PNS) calcium signaling

Significance

The increase in obesity has been accompanied by a rise in the prevalence of peripheral neuropathy. Because there is no disease-modifying therapy, paradigm-shifting research on pain associated with obesity, metabolic syndrome, and type 2 diabetes is urgently needed. Our data suggest that fecal transplantation from lean to obese, insulin-resistant mice decreases obesity-induced hypersensitivity and increases nerve density in the skin. These improvements are accompanied by changes in peripheral nerve system gene expression and inflammatory cells. Finally, our results suggest that circulating butyrate, a metabolite secreted by gut microbiome and absorbed in the blood stream, may be involved by acting directly on peripheral nerve system immune cells and gene expression or pain channels.

and immune cells concurrent to FMT-induced pain improvement. Furthermore, our results point to modulation of circulating butyrate as one of the underlying causes of this improvement in rodents. In parallel studies, we identified an association between lower circulating butyrate and distal pain in obese humans. The gut microbiome, circulating butyrate, and its downstream pathways in the PNS may represent novel targets for disease-modifying therapy.

Results

FMT Improves Obesity-Induced Hypersensitivity. We hypothesized that reshaping the gut microbiome of mice fed a WD would alleviate indices of neuropathic pain. We therefore subjected mice to a 12-wk WD feeding paradigm known to cause mechanical allodynia and thermal hyperalgesia (7) (Fig. 1 *C* and *D*, left side of dashed line, and *SI Appendix*, Fig. S1 *A–C*). To better characterize the WD-fed model, we performed 16S analysis of fresh feces and cecal content. WD-fed mice exhibited a poorer bacterial diversity compared to lean, normal chow (NC)-fed mice, as represented by lower α-diversity index (unpaired t test, $P = 2.7224e-05$) (*SI Appendix*, Fig. S1*D*). In addition, WD reduced the abundance of butyrate-producing bacteria of the genera *Lactobacillus* and *Lachnospiraceae* (unpaired t test, $P = 0.0107$ and $P = 0.0174$, respectively) *SI Appendix*, Fig. S1 *E and F*) in comparison to NC-fed animals.

We performed FMT on WD-fed obese mice and generated many other groups to test multiple variables individually. Following 12 wk on WD, all obese mice were subjected to a regimen of 3 d of broad-spectrum antibiotic treatment (ABX) (Fig. 1*A*). We chose the minimum time and dose of antibiotic treatment necessary to deplete bacteria present in the feces (one-way ANOVA with repeated measures $P = 0.0072$, Tukey's post hoc pre-ABX vs. post-ABX $P = 0.0315$, pre-ABX vs. post-FMT $P = 0.9196$, and post-ABX vs. post-FMT $P = 0.0189$) (Fig. 1*B*), as extended periods of antibiotic exposure can modify nerve function and myelination (33). After antibiotic treatment, we initiated the 2-wk FMT paradigm, which also included a diet switch (DS). For the DS, some WD-fed, obese mice were switched to NC diet during the first 5 d of saline (sham FMT) or fecal slurry from lean mice (FMT) gavage. The rationale, motivated by previous literature (34–37), was to allow for colonization of the gut with bacteria thriving in NC rather than WD conditions. Importantly, both sham FMT- and FMT-treated mice had similar amounts of cecal bacterial DNA at endpoint (unpaired t test $P = 0.845$) (*SI Appendix*, Fig. S2*A*).

Of mice that did not receive antibiotics and subsequent gavage, WD-fed mice developed significant allodynia compared to mice fed standard diet ($P < 0.05$ by unpaired t test) (Fig. 1*C*, left side of dashed line). Of the groups that received antibiotics (Fig. 1*C*, right side of dashed line), animals gavaged with saline (S) showed the highest mechanical allodynia (lowest threshold), irrespective of whether they underwent DS or not. Both groups subjected to the fecal transplantation from lean mice (with or without DS) showed significantly higher paw withdrawal thresholds compared to their counterparts (two-way ANOVA, main
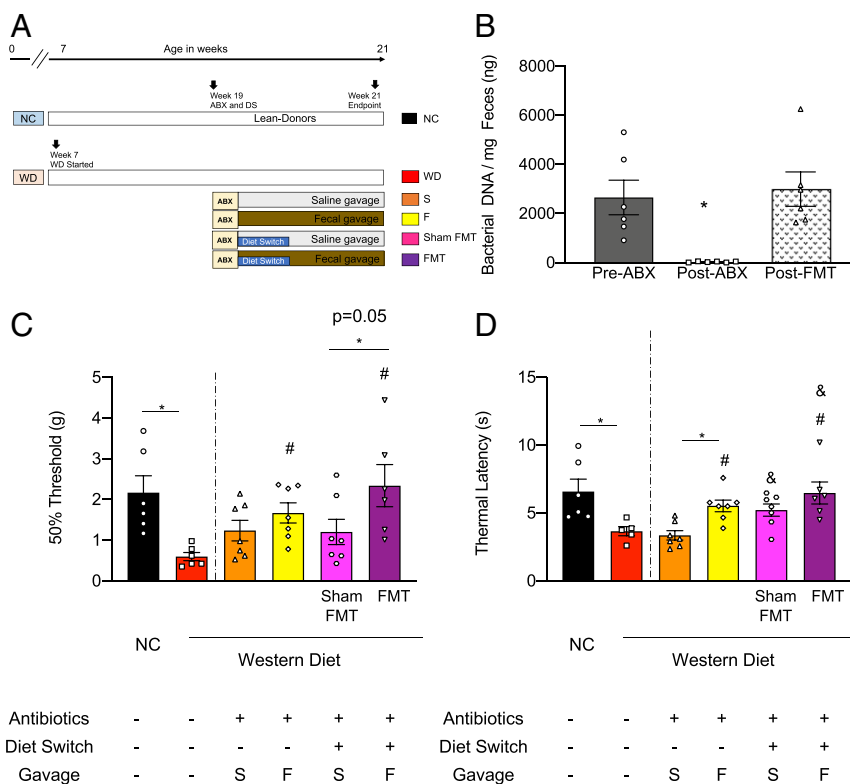

Fig. 1. FMT improves obesity-induced hypersensitivity. (*A*) Paradigm schematic; NC, WD, antibiotics (ABX), diet switch (DS), saline gavage (S), lean feces gavage (F), sham FMT (WD, ABX, DS, S), FMT (WD, ABX, DS, F). (*B*) Bacterial DNA quantification before and after antibiotics exposure (pre-ABX and post-ABX, respectively) and after FMT treatment (post-FMT). (*C*) Mechanical allodynia and (*D*) thermal hyperalgesia in NC- and WD-fed mice [controls, no treatment, left side of dashed lines; $P = 0.0044$, and $P = 0.0214$, for mechanical (*C*) and thermal hypersensitivities (*D*), respectively, by unpaired t test], and in WD-fed mice subjected to antibiotics with (+) or without (−) DS, S gavage, or feces from lean mice gavage (F) (right side of the dashed lines). Two-way ANOVA main effect of FMT treatment, #$P = 0.0282$, Sidak post hoc *$P = 0.05$ between sham FMT and FMT for (*C*) mechanical allodynia. Two-way ANOVA main effect of FMT treatment #$P = 0.003$ and main effect of DS &$P = 0.012$, Sidak post hoc *$P = 0.01$ for (*D*) thermal hyperalgesia. All values represent mean± SEM, ($n = 6$–7 per group).

effect of FMT, $^\#P = 0.0282$, Sidak post hoc $^*P = 0.05$ between sham FMT and FMT).

Of mice that did not receive antibiotics and subsequent gavage, WD-fed mice developed significant heat hyperalgesia compared to mice fed standard diet ($P < 0.05$ by unpaired t test) (Fig. 1*D*, left side of dashed line). Of the groups that received antibiotics (Fig. 1*D*, right side of dashed line), animals gavaged with S that did not undergo DS showed the highest thermal sensitivity (lowest latency). Lean feces transplantation (F) without DS significantly increased heat-response latency compared to that of obese mice subjected to ABX treatment, without DS, and S gavage (Sidak post hoc, $P = 0.01$). Animals that received DS and S gavage (sham FMT) had an increase in thermal latency as well. DS also potentiated the positive effect of gavaging feces from lean to obese mice on thermal hypersensitivity (two-way ANOVA, all groups showed a main effect of FMT treatment $^\#P = 0.003$ and also a main effect of diet switch $^\&P = 0.012$). Our results suggest that fecal transplantation of fecal slurry from lean to WD-fed, obese mice (previously exposed to 3 d of antibiotic) prevented mechanical allodynia and thermal hyperalgesia. Additionally, a DS at the beginning of the gavage procedure tended to potentiate the positive effects of lean feces transplantation on pain behaviors. None of these treatments decreased the animals' body weight (*SI Appendix*, Fig. S2*B*). However, in our model and as published by many authors (38–40), fasting glucose was slightly lower after FMT in comparison to sham FMT, but significantly lower when compared to WD-fed, antibiotics-treated, S-gavaged mice that did not receive DS (two-way ANOVA showed a main effect of FMT gavage $^\#P = 0.0042$; Sidak post hoc, $^*P = 0.04$) (*SI Appendix*, Fig. S2*C*). Interestingly, this decrease in fasting glucose did not correlate with improved pain, suggesting that other mechanisms were involved (Pearson's $r = -0.24$) (*SI Appendix*, Fig. S2*D*).

Behavioral measurements were also made in cohort of mice treated with antibiotics only (no gavage and no DS) (*SI Appendix*, Fig. S3). NC-fed mice presented altered both mechanical threshold (unpaired t test $P = 0.0244$) (*SI Appendix*, Fig. S3*A* and S3*E*) and thermal latency (unpaired t test $P = 0.0068$) (*SI Appendix*, Fig. S3*C* and S3*F*) following antibiotics exposure. A 3-d antibiotic treatment, performed 2 wk before any measurements, increased mechanical threshold in WD-fed mice (unpaired t test $P = 0.0256$) (*SI Appendix*, Fig. S3*B* and S3*E*). In contrast, thermal latency was unchanged in ABX-treated animals fed WD (unpaired t test $P = 0.3316$) (*SI Appendix*, Fig. S3*D* and S3*F*). These data suggest that even a short antibiotics treatment may modify mechanical sensitivity differently in obese mice and will need to be followed-up. However, the paradigm—antibiotics, gavage of fecal slurry from lean mice, accompanied by a short DS during the first days (called FMT in the present study)— exhibited the greatest pain improvement in WD-fed mice.

FMT Alters Transcripts in Dorsal Root Ganglia and Sciatic Nerve. To understand the cause of pain relief by FMT, we performed RNA-sequencing analysis on the dorsal root ganglia (DRG) and sciatic nerve (SN) of sham FMT and FMT obese animals. Eighty-two mRNA levels were different in the DRG of FMT mice compared to sham FMT (Fig. 2*A* and Dataset S1). Among them were transcripts involved in: 1) Epigenetic modifications, such as lysine-specific methyltransferase 2A (*KMT2A*); 2) calcium release from the endoplasmic reticulum (ER) and the ryanodine receptor 2 (*RYR2*); 3) lipid metabolism, including ATP-binding cassette A1 (*ABCA1*) and apolipoprotein E (*ApoE*); 4) and mechanosensory pathways, such as *PIEZO2*, all of which were down-regulated in the DRG of FMT-treated mice compared to sham FMT (Dataset S1). Interestingly it has been shown that epigenetic regulators could play a role in neuropathic pain (41). Calcium handling and lipid metabolism transcripts had also previously been shown to be altered in peripheral neuropathy (6, 42). Moreover, the mechanosensory gene

PIEZO2 had been linked to inflammation-mediated mechanical allodynia (43). Metascape pathway analysis (q value < 0.05) revealed changes in neuronal morphogenesis, sensory perception of pain, behavioral response to pain, and calcium handling among the topmost regulated pathways in the DRG following FMT intervention (Fig. 2*C*). These data suggest that FMT alters DRG neuronal growth, hyperexcitability and pain response.

Thirty-nine mRNAs were significantly differentially regulated when comparing the SN of FMT- and sham FMT-treated mice (Fig. 2*B* and Dataset S2). Obese mice subjected to FMT showed decrease in immunoregulatory transcripts (Dataset S2), including cytokine-like 1 (*CYTL1*), previously described in monocyte/macrophage recruitment (44), and IL-33 (*IL33*), known to be involved in tissue repair. Interestingly, FMT also decreased expression levels of γ-aminobutyric A receptor subunit α3 (*GABRA3*) transcripts (Dataset S2). Activation of GABA$_A$ ionotropic channels had been demonstrated to reverse neuropathic hypersensitivity (45). Metascape analysis (Fig. 2*D*) indicated dysregulation of noncanonical Wnt and bone morphogenetic protein pathways known to sensitize nociceptors (46, 47) and of insulin-like growth factor pathways that have been shown to increase neuronal excitability via enhancing calcium currents and, thus, increase pain sensitivity (48), as well as to stimulate mononuclear cell migration in a model of rheumatoid arthritis (49). Our data indicate that FMT modifies specific transcripts in the nerve, such as immune regulatory response, potentially underlying pain alleviation.

FMT Decreases RYR2-Dependent Calcium Release from the ER of DRG Neurons. To better understand the neurobiology of our model, we performed RNA sequencing in the DRG and SN of NC- and WD-fed mice. A total of 4,280 transcripts were differentially expressed in the DRG between NC- and WD-fed mice (Dataset S3). Choline acetyltransferase (*ChAT*) and solute carrier family 18 member A3 (*Slc18a3*)—also known as vesicular acetylcholine transporter (*VAChT*)—were the two topmost up-regulated genes in the DRG of WD-fed compared to NC-fed mice (*SI Appendix*, Fig. S4*A*). This suggested WD-induced activation of muscarinic receptor signaling, a pathway known to confer neuroprotective effects in peripheral neuropathy when therapeutically blocked (50). The up-regulated pathways in the DRG of WD- compared to NC-fed animals involved pathways comprising many genes that regulate neuronal excitability (*SI Appendix*, Fig. S4*B*), while a majority of the down-regulated pathways in the DRG of WD-fed mice represented inflammatory responses, cytokine production, neutrophil degranulation, and leukocyte migration (*SI Appendix*, Fig. S4*C*).

To understand whether FMT improved neuropathic pain by potentially rescuing some of the WD-induced changes in the PNS or by increasing FMT-specific pathways, we sought to identify the genes that were inversely changed in WD- versus NC-fed mice compared to FMT versus sham FMT animals. RYR2, a protein that regulates calcium release from the ER to the cytoplasm, was significantly increased in the DRG of WD-fed mice compared to that of NC-fed animals (false-discovery rate [FDR]-adjusted $P = 8.30E-08$) (Fig. 3*A*) and decreased after FMT intervention when compared to sham FMT (FDR-adjusted $P = 0.00433$) (Fig. 3*B*). This led us to investigate the caffeine-induced calcium transient response (RYR2-dependent release of calcium from the ER) in neurons from the DRG of NC-fed, obese control, and FMT-treated mice. We purified and cultured DRG neurons from mice from the aforementioned groups and measured the ER calcium release postcaffeine stimulation, as represented in Fig. 3*C*. Neurons cultured from WD-fed animals showed a higher calcium release from the ER following caffeine stimulation (Fig. 3*D*) when compared to neurons isolated from NC-fed mice. These data suggest a greater calcium release by the ER that could potentially underlie neuronal hyperexcitability and high intracellular calcium observed in WD-fed neurons, as published in the past (13). Noticeably, neurons from
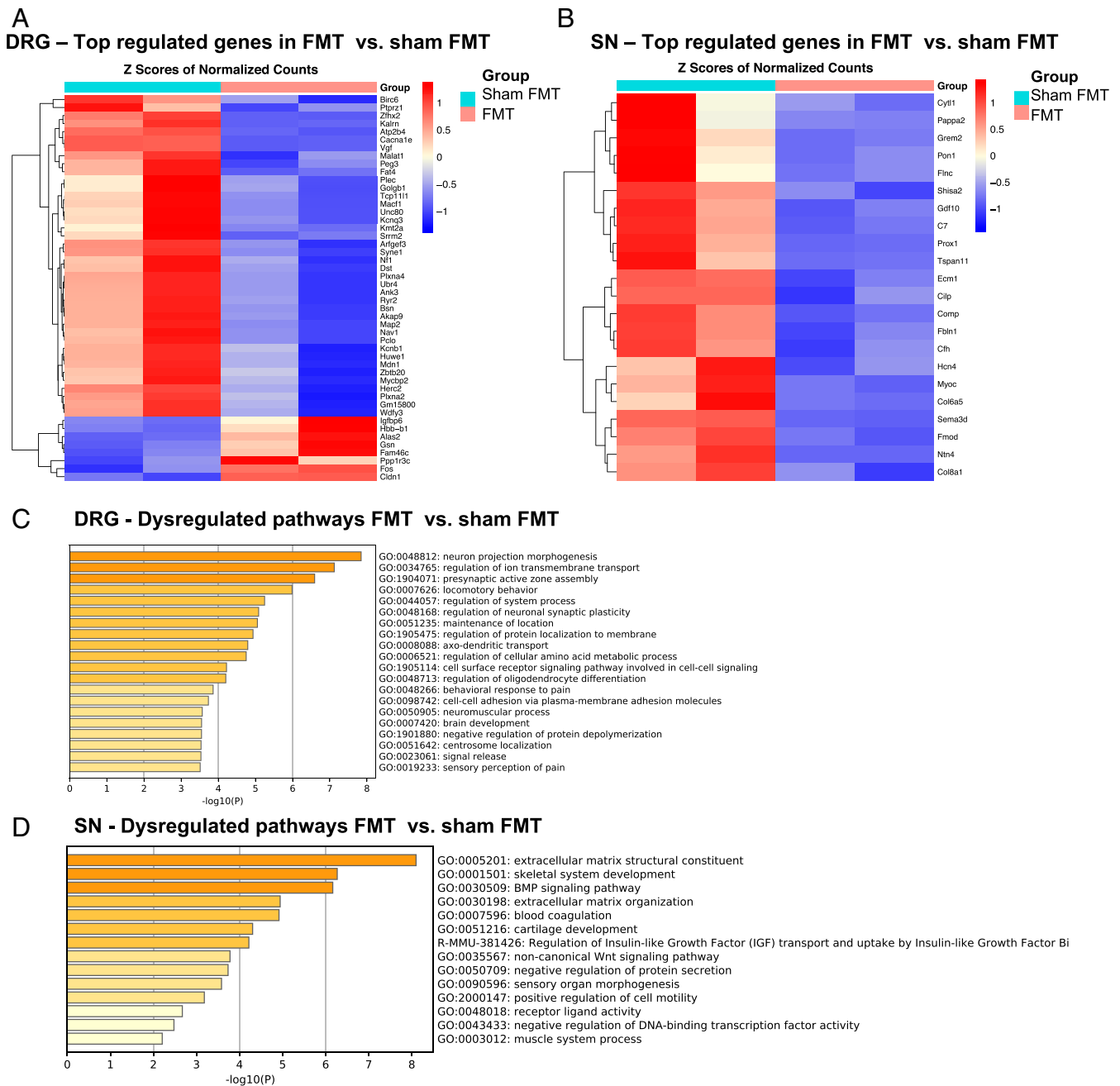
A

DRG – Top regulated genes in FMT vs. sham FMT

Z Scores of Normalized Counts

Group
Sham FMT
FMT

Birc6, Ptprz1, Zfhx2, Kalrn, Atp2b4, Cacna1e, Vgf, Malat1, Peg3, Fat4, Plec, Golgb1, Tcp11l1, Macf1, Unc80, Kcnq3, Kmt2a, Srrm2, Arfgef3, Syne1, Nf1, Dst, Plxna4, Ubr4, Ank3, Ryr2, Bsn, Akap9, Map2, Nav1, Pclo, Kcnb1, Huwe1, Mdn1, Zbtb20, Mycbp2, Herc2, Plxna2, Gm15800, Wdfy3, Igfbp6, Hbb–b1, Alas2, Gsn, Fam46c, Ppp1r3c, Fos, Cldn1

B

SN – Top regulated genes in FMT vs. sham FMT

Z Scores of Normalized Counts

Group
Sham FMT
FMT

Cytl1, Pappa2, Grem2, Pon1, Flnc, Shisa2, Gdf10, C7, Prox1, Tspan11, Ecm1, Cilp, Comp, Fbln1, Cfh, Hcn4, Myoc, Col6a5, Sema3d, Fmod, Ntn4, Col8a1

C   **DRG - Dysregulated pathways FMT vs. sham FMT**

GO:0048812: neuron projection morphogenesis
GO:0034765: regulation of ion transmembrane transport
GO:1904071: presynaptic active zone assembly
GO:0007626: locomotory behavior
GO:0044057: regulation of system process
GO:0048168: regulation of neuronal synaptic plasticity
GO:0051235: maintenance of location
GO:1905475: regulation of protein localization to membrane
GO:0008088: axo-dendritic transport
GO:0006521: regulation of cellular amino acid metabolic process
GO:1905114: cell surface receptor signaling pathway involved in cell-cell signaling
GO:0048713: regulation of oligodendrocyte differentiation
GO:0048266: behavioral response to pain
GO:0098742: cell-cell adhesion via plasma-membrane adhesion molecules
GO:0050905: neuromuscular process
GO:0007420: brain development
GO:1901880: negative regulation of protein depolymerization
GO:0051642: centrosome localization
GO:0023061: signal release
GO:0019233: sensory perception of pain

-log10(P)

D   **SN - Dysregulated pathways FMT vs. sham FMT**

GO:0005201: extracellular matrix structural constituent
GO:0001501: skeletal system development
GO:0030509: BMP signaling pathway
GO:0030198: extracellular matrix organization
GO:0007596: blood coagulation
GO:0051216: cartilage development
R-MMU-381426: Regulation of Insulin-like Growth Factor (IGF) transport and uptake by Insulin-like Growth Factor Bi
GO:0035567: non-canonical Wnt signaling pathway
GO:0050709: negative regulation of protein secretion
GO:0090596: sensory organ morphogenesis
GO:2000147: positive regulation of cell motility
GO:0048018: receptor ligand activity
GO:0043433: negative regulation of DNA-binding transcription factor activity
GO:0003012: muscle system process

-log10(P)

Fig. 2. FMT alters transcripts in the DRG and SN. (*A*) Topmost regulated transcripts after FMT in the DRG (sham FMT = ABX, DS, S gavage; FMT = ABX, DS, gavage of fecal slurry from lean mice). (*B*) Topmost regulated transcripts after FMT in the SN. (*C*) Metascape pathway analysis of dysregulated genes in the DRG. (*D*) Metascape pathway analysis of dysregulated genes in the SN. FDR-adjusted $P < 0.05$ ($n = 2$ biological replicates, each replicate = 6 lumbar DRG and 2 SN). (Datasets S1 and S2).

FMT-treated animals showed a decrease in the amplitude of caffeine-induced calcium transient in comparison to WD-fed–only animals (Fig. 3*D*). These data demonstrate that neurons from obese mice had higher calcium release from the ER, associated with a higher expression of *RYR2* in DRG neurons, whereas the DRG from mice subjected to FMT had a lower caffeine response, suggesting lower neuronal ER excitability when compared to WD-fed animals, potentially due to decreased *RYR2* expression in the ER.

FMT Alters Macrophage Polarization within the DRG and SN Compared to Autologous FMT. It is well established that immune cells and activated nociceptors orchestrate a neural reflex circuitry (51–53).

Moreover, peripheral monocytes and macrophages have a crucial role in enhancing or dampening hypersensitivities in pain models (54). In a separate cohort, we performed flow cytometry to study immune cells within the DRG and SN of FMT versus autologous FMT (auto FMT)-treated mice. Autologous fecal gavage, consisting of fecal transplantation from obese to obese mice, was done to rule out an effect of fecal gavage on inflammation.

We used a specific set of cell surface markers to identify myeloid cell population and M1/M2 macrophage polarization. The gating strategy utilized is shown in *SI Appendix*, Fig. S5*A*. We observed an increase in percentage of M2 macrophages (CD45^{+hi}CD11B^{+}CD206^{+}) within the DRG of FMT mice when
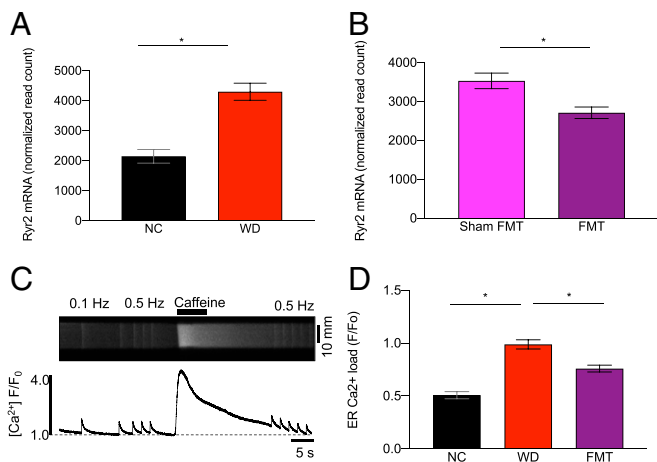
Fig. 3. FMT decreases RYR2-dependent calcium release from the ER of DRG neurons. (*A*) *RYR2* mRNA levels in WD- versus NC-fed mice (FDR-adjusted $P = 8.30E-08$) and (*B*) in FMT versus sham FMT-treated animals (FDR-adjusted $P = 0.00433$) ($n = 2$ biological replicates, as shown Fig. 2). (*C*) Representative image of caffeine-induced calcium release from the ER. (*D*) Quantitation of ER-calcium load in neurons from NC-, WD-, and FMT-treated mice ($n = 20-25$ cells from 3 animals for each conditions). All values represent mean ± SEM, *$P < 0.05$.

compared to auto FMT animals (unpaired *t* test, $P = 0.0396$) (Fig. 4*A*). Interestingly, we observed a decrease in percent of M2 macrophages within the SN of FMT-treated mice in comparison to auto FMT (unpaired *t* test, $P = 0.0507$) (Fig. 4*B*). These results indicate a shift toward alternative activation of macrophages—with an antiinflammatory/tissue repair phenotype—within the DRG of obese mice transplanted with feces from lean animals. Of note, FMT mice showed improvement in mechanical allodynia when compared to auto FMT-treated animals (unpaired *t* test $P = 0.0436$) (*SI Appendix*, Fig. S5*B*).

FMT Increases Nerve Density in the Skin of Obese Mice. In neuropathy models, inflammation is often linked to papillary dermal and intraepidermal nerve fiber (IENF) densities (55). We observed that the WD-fed animals had fewer skin fibers compared to NC-fed mice (unpaired *t* test $P = 0.0149$ and $P < 0.0001$) (Fig. 5 *A* and *B*, left side of dashed lines). We also counted fibers in the hind paws of FMT- and auto FMT-treated mice. FMT mice had a higher nerve density in the papillary dermis when compared to auto FMT mice (unpaired *t* test $P = 0.0451$) (Fig. 5*A*, right side of dashed line). However, both groups showed a similar IENF density (unpaired *t* test $P = 0.7618$) (Fig. 5*B*, right side of dashed line). These data indicate that the FMT paradigm impacted dermal nerve density, suggestive of either attenuation of the rate of distal degeneration or nerve regeneration.

Nerve densities were also measured in mice treated with antibiotics only (*SI Appendix*, Fig. S6). Interestingly, antibiotic treatment alone did not have an effect on either dermal or IENF densities in NC-fed animals (unpaired *t* test $P = 0.1544$, and $P = 0.1331$, respectively) (*SI Appendix*, Fig. S6 *A, C, E,* and *F*). However, WD-fed mice subjected to antibiotic exposure had a decrease in number of both dermal and epidermal fibers when compared to WD control animals (unpaired *t* test $P = 0.0043$, and $P = 0.0029$, respectively) (*SI Appendix*, Fig. S6 *B* and *D–F*). Thus, brief antibiotic exposure affected nerve densities of obese mice and will need to be followed-up in future experiments.

Butyrate Correlates with Mechanical Allodynia Improvement, Modifies DRG Immune Cell Activation, and DRG Gene Expression. Our data demonstrated that FMT improved WD-induced neuropathic pain

and potentially modified neuronal excitability and PNS immune cells. Therefore, we sought to identify components of the microbiome that could directly lead to some of the gene reprogramming and immune cell changes in the PNS. Metascape analysis (*q* value < 0.05) identified lipid metabolism pathways to be up-regulated in the SN of WD-fed mice compared to NC-fed animals (*SI Appendix*, Fig. S7*A*). Moreover, one of the topmost dysregulated transcripts in the SN between NC- and WD-fed animals was free fatty acid receptor 2 *(FFAR2)*. *FFAR2* transcript was identified as being increased by 25-fold in the SN of WD-fed compared to NC-fed mice (*SI Appendix*, Fig. S7*B* and Dataset S4). FFAR2 is a G coupled-protein receptor that binds to short-chain fatty acids (SCFA) and is expressed by immune cells (56). SCFA include acetate, butyrate, propionate, and valerate and are produced by the gut microbiome and pass into the blood stream (34–36, 40, 57–60). We previously identified a negative correlation between plasma butyrate and body mass index (BMI) in humans (61). Reports suggest that butyrate may improve health (62–65) and lead to improvement of pain behaviors in models of nerve injury-induced pain (66), but the molecular mechanisms are not known. Thus, we evaluated the levels of butyrate in the plasma of sham FMT- and FMT-treated mice and observed that FMT intervention led to a significant increase in the serum levels of butyrate (Mann–Whitney *U* test, $P = 0.0411$) (Fig. 6*A*).

Given the potential link between butyrate and pain, we hypothesized that increasing butyrate in the blood of WD-fed mice may improve WD-induced hypersensitivity. We tested various routes of butyrate treatment, doses, and drug compounds. We needle-fed obese, hypersensitive mice with tributyrin (three butyrate molecules with a glycerol backbone) or glycerol (used as vehicle) for 2 wk and observed an increase in circulating butyrate in blood of tributyrin-treated mice (unpaired *t* test, $P = 0.0264$) (*SI Appendix*, Fig. S8*A*). Mechanical and thermal hypersensitivities of WD-fed mice supplemented with tributyrin were also analyzed. Using a median-based threshold, we selected mice with the best pain phenotype and performed linear regression analysis. We observed a positive correlation between plasma levels of butyrate and 50% paw withdrawal threshold (Pearson's $r = 0.8145$) (Fig. 6*B*), but not between thermal latency (Pearson's $r = -0.3276$) (*SI Appendix*, Fig. S8*B*). Our results suggest that the increase in circulating butyrate after FMT intervention and tributyrin treatment may be involved in pain alleviation.

SCFA, and especially butyrate, have been described to modulate innate and adaptive immune response via immune cell recruitment, proliferation, and activation, as well as regulation of cytokine and chemokine production (67–69). Butyrate has also been shown to increase extrathymic regulatory T (Treg) cell population in vitro and in vivo (24, 25). Tregs are immune-suppressive and have an important role in maintaining immune tolerance. Thus, we analyzed immune cell activation levels within
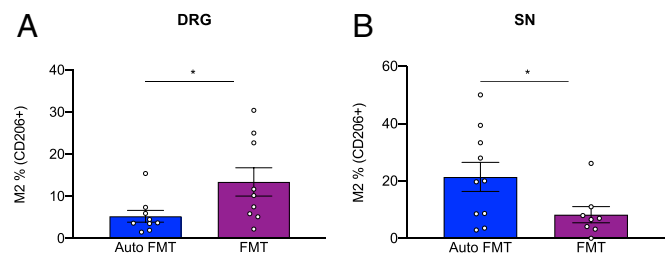

Fig. 4. FMT alters macrophage polarization within the DRG and SN compared to auto FMT. (*A*) Percent of M2 macrophages within the DRG of auto FMT (obese mice gavaged with feces from obese animals) versus FMT-treated mice (unpaired *t* test, $P = 0.0396$). (*B*) Percent of M2 macrophages within the SN of auto FMT- vs. FMT-treated mice (unpaired *t* test, $P = 0.0507$; $n = 8-10$). All values represent mean ± SEM, *$P < 0.05$.
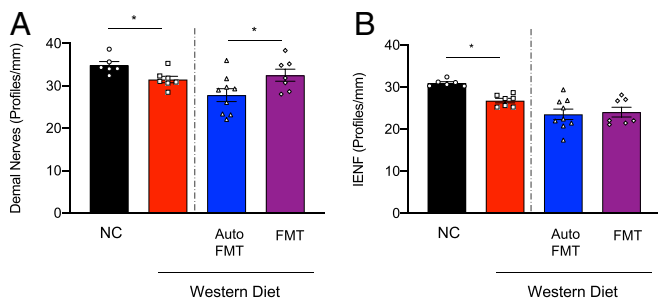
Fig. 5. FMT increases nerve density in the skin of obese mice. (A) Dermal nerve density from NC- vs. WD-fed mice (unpaired *t* test, left side of dashed line; *P* = 0.0149), and auto FMT- vs. FMT-treated mice (unpaired *t* test, *r*ight side of dashed line; *P* = 0.0451) (*n* = 6–10 per group). (B) IENF of NC- vs. WD-fed mice (unpaired *t* test, left side of dashed line; *P* < 0.001) and from auto FMT- and FMT-treated animals (unpaired *t* test, right side of dashed line; *P* = 0.07618). (*n* = 6–10 per group). All values represent mean ± SEM, *P* < 0.05.

the DRG and SN of tributyrin-treated obese animals using CD45 as a pan-leukocyte marker. Tributyrin treatment decreased leukocyte activation levels in the DRG of obese mice (unpaired *t* test, *P* = 0.001) (Fig. 6*C*) as represented by the lower CD45 mean intensity fluorescence, but not in the SN (unpaired *t* test, *P* = 0.532) (*SI Appendix*, Fig. S8*C*).

Butyrate is known to have an epigenetic role by altering histone deacetylase (HDAC) function in many cell types (70). Given our data, we hypothesized that butyrate treatment may directly change *HDAC* gene expression in DRG explants (containing neurons, satellite, glial, and immune cells). Sodium butyrate-treated (5 µM) DRG explants showed an increase in *HDAC2* mRNA expression levels when compared to vehicle-treated DRG explants (unpaired *t* test, *P* = 0.01) (Fig. 6*D*). This result indicates that butyrate can directly modify *HDAC2* mRNA levels in mouse DRG cells and alter gene expression.

Butyrate Modulates TRPV1 Activity as a Partial Agonist In Vitro. Transient receptor potential cation channel subfamily vanilloid 1 (TRPV1) is a nonselective cation channel that mediates calcium influx, resulting in sensitization of nociceptive neurons, generation of action potentials and, ultimately, pain sensation (71). TRPV1 had been shown to be modulated by a variety of endogenous ligands, including some peptide hormones and small lipids (72).

We measured butyrate-evoked TRPV1 activation in a heterologous expression system. Butyrate alone did not result in profound activation of TRPV1 but preactivation of channels with capsaicin primed strong TRPV1 activation when butyrate was subsequently applied, regardless of whether capsaicin was still present (Fig. 7*A* and *D*) (two-way RM ANOVA, with pairwise Tukey post-hoc test, V1 capsaicin vs V1-butyrate 1, prob>|t| = 0.00622 and V1-butyrate2 vs. V1-butyrate1, prob>|t| = 0.00977). Control studies using cells not expressing TRPV1 confirmed this to be TRPV1-dependent (Fig. 7*C*). Furthermore, brief exposure to low pH conditions primed a marked TRPV1 response to butyrate (Fig. 7 *B* and *E*) (two-sample *t* test of summarized data, *P* = 0.00532). These results suggest that butyrate acts as a partial agonist of TRPV1 channels.

We next investigated whether butyrate enhanced TRPV1 desensitization and thus could exert modulatory effects during
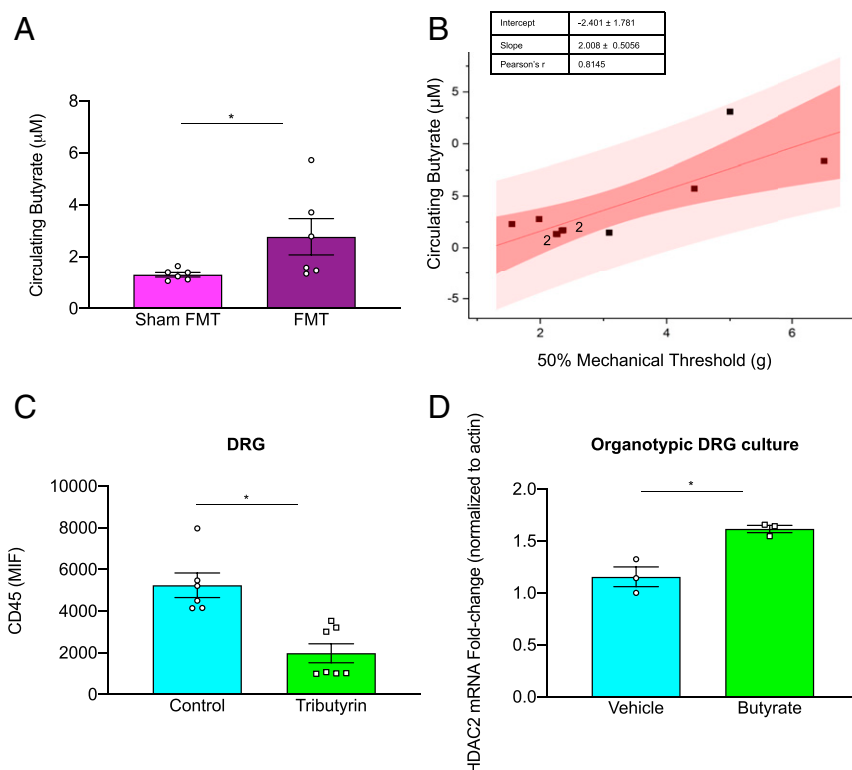
Fig. 6. Butyrate correlates with mechanical allodynia improvement, modifies DRG immune cell activation, and DRG gene expression. (A) Serum butyrate concentration of sham FMT- and FMT-treated mice (Mann–Whitney *U* test, *P* = 0.0411). (B) Linear regression and Pearson correlation between 50% paw withdrawal threshold and serum butyrate concentration (numeral 2 represents the number of undistinguishable, overlapping samples; Person's *r* = 0.8145). (C) CD45 mean intensity fluorescence (MIF) in the DRG from control and tributyrin-treated mice (unpaired *t* test, *P* = 0.001; *n* = 8–10 per group). (D) *HDAC2* mRNA fold-change normalized to actin from vehicle and butyrate treated organotypic DRG cultures (unpaired *t* test, *P* = 0.01; *n* = 3 per condition). All values represent mean ± SEM, *P* < 0.05.

inflammatory pain. When capsaicin was consecutively applied at subsaturating levels in the absence of butyrate, the second response was ~23% lower than the first response (Fig. 7F). Interestingly, when low (5 μM) but not moderate (50 μM) concentrations of butyrate were coapplied with capsaicin, the degree of desensitization observed with subsequent capsaicin administrations significantly increased (Fig. 7 G–I) (one-way ANOVA, with Bonferroni post-hoc test, 0 μM vs. 5 μM, t = 0.01651, α = 0.05). These findings implicate butyrate as a partial agonist of TRPV1 that dose-dependently modulates the active state of channel function.

These data implicate circulating butyrate in changing PNS sensitivity via a direct action on TRPV1 channels.

Serum SCFA and Distal Pain in Humans. Our results led us to examine the association between circulating butyrate, distal pain, and sensory loss in obese individuals. To explore this hypothesis, we assessed peripheral pain in a subset of 29 participants currently enrolled in the METS (Modeling the Epidemiologic Transition Study)-Microbiome study (56) in which obesity risk factors, gut microbiota, and SCFA are prospectively evaluated (Table 1). We used the Utah Early Neuropathy Scale (UENS) (57) to evaluate sensory loss and NeuroQol (NQOL) questionnaire (58) to evaluate the pain phenotype. Participants with a NeuroQol score > 3 on selected questions (as described in *Materials and Methods*) were categorized as presenting "distal pain." Serum SCFAs levels were adjusted for participants' body weight. Overall, participants with distal pain tended to have lower circulating SCFAs, including butyrate (P = 0.1401), propionate (P = 0.1681), acetate (P = 0.1923), and valerate (0.0854) (Tables 2 and 3). Sensory loss assessed using the UENS scoring did not show any trends. These findings will need to be followed-up with more participants but suggest that obese individuals starting to develop distal pain might benefit from personalized treatments (e.g., butyrate, SCFA) or dietary plan (e.g., containing fibers) aiming at increasing serum levels of SCFA.

Discussion

This study demonstrated that FMT can reverse early indices of sensory nerve dysfunction induced by a WD. Our data suggest that FMT and potentially a metabolite secreted by the gut microbiome in the bloodstream, butyrate, alter gene expression in PNS cells (neurons, macrophages, and Schwann cells) to modify neuronal hyperexcitability and immune cells of the PNS. Identifying a mechanism linking the gut microbiome with modulation of the peripheral neuroimmune system offers the possibility of developing targeted therapeutic interventions to prevent onset of peripheral neuropathy in prediabetes and reverse established neuropathy in patients with prediabetes and type 2 diabetes.

It is well established that diet-induced obesity murine models and human obesity are associated with gut dysbiosis (73–78). Notably, the gut microbiome has recently been linked to pain (28–30, 66, 79) but to date has not been associated with pain in obesity models. In the present study, we showed that FMT from lean to WD-fed mice improved both mechanical allodynia and thermal hyperalgesia without changing body weight. FMT-treated obese animals also had higher nerve density in the skin. Loss of distal sensory nerves is a measure of sensory neuropathology noted in both WD-fed mice (13) and humans with metabolic syndrome (80, 81). It was particularly notable that while WD reduced density of both epidermal (IENF) and dermal nerves, FMT impacted only dermal nerve density. This is suggestive either of attenuation of the rate of distal degeneration that is associated with loss of sensory nerves in the skin by FMT or initiation of regeneration from proximal regions of nerve, but not of collateral sprouting from residual epidermal fibers.

The coexistence of sensory fiber loss with neuropathic pain and the capacity of interventions that promote neuroprotection and regeneration of fibers to alleviate indices of pain has also been reported in animals and humans with diabetic peripheral neuropathy (42) and chemotherapy-induced peripheral neuropathy (82, 83). A recent study has shown that gut bacteria eradication by a longer antibiotic treatment paradigm prevented development of mechanical hyperalgesia in a model of chemotherapy-induced pain (30). Additionally, antibiotics exposure did not have an effect in thermal latency in WD-fed mice, but it increased thermal threshold in NC-fed animals. Antibiotics treatment had been linked to increased risk of peripheral neuropathy and to nerve damage (84), especially associated with comorbidities such as obesity. Thus, it is interesting that in our model, modulation of gut microbiome by a brief period of large-spectrum antibiotics led to mechanical hyperalgesia in NC-fed animals but improved mechanical allodynia in obese mice.

Studies have shown that WD-induced hypersensitivity can be explained by neuron hyperexcitability arising from an increase in intracellular calcium flux in response to low concentrations of nociceptor activators (13). RYRs, including RYR2, have been linked with pain (85, 86). These ER-associated receptors, widely studied in the heart, have been shown to regulate release of peptide-containing vesicles following intracellular calcium release (87, 88). Our present study suggests a key role of RYR2 expressed by nociceptors in WD-induced painful neuropathy and also in the FMT-induced improvement. We, together with others, have previously shown that ER stress in nociceptor is one of the first events occurring in WD-induced hypersensitivity (7, 89). This ER stress may result in changes in *RYR2* expression or in abnormal calcium handling in neurons and subsequent hypersensitivity (89, 90). Our data identified neural *RYR2* as potentially involved in obesity-associated pain and in the efficacy of FMT. Manipulation of RYR2 expression in PNS cell types using cre-lines and evaluation of live calcium handling in PNS cell types may allow the regulation of RYR2 by butyrate and its potential as drug target to be studied.

The efficacy of FMT may result from actions on PNS immune cells. The down-regulation of immune regulatory transcripts in the SN from FMT-treated mice suggests that modulation of the gut microbiome and its metabolites impacts immune mechanisms that mediate nociceptor sensitization. Cytokines such as IL-1β can mediate pain sensitization by altering neuron excitability and increasing neuronal firing, leading to increased mechanical and thermal sensitivities (51). Peripheral macrophages have been implicated in the development of mechanical allodynia (91) and M2-polarized macrophages have been associated with wound healing and antiinflammatory function (92). A recent study also pointed to the role that DRG macrophages, but not macrophages located at the injury site, have in peripheral pain initiation and maintenance in a model of nerve injury (93). The lower percentage of M2 macrophages within the SN in our model suggests that the termination of inflammatory response associated with these immune cells is initiated locally in the DRG, where the neuronal cell bodies are located and where we observed an increase in percent of M2 macrophages following FMT intervention.

A recent report showed that transcriptional changes in the DRG caused by nerve injury correlated with temporal changes in nocifensive behavior: Changes observed in nociceptor-related transcripts correlated with the early development of cold allodynia, while changes observed in immune-related genes correlated with the later development of tactile allodynia (91). These findings may be pertinent to the differences we observed in normalization of mechanical and thermal sensitivities after DS and FMT.

The relationship between the gut microbiota, its derived metabolites, especially butyrate, and neurological diseases, including pain, has received increasing attention in recent years. Circulating butyrate, acetate, and propionate are mainly derived from gut microbiota, although small quantities are also produced by humans as products of protein metabolism (94). These SCFA
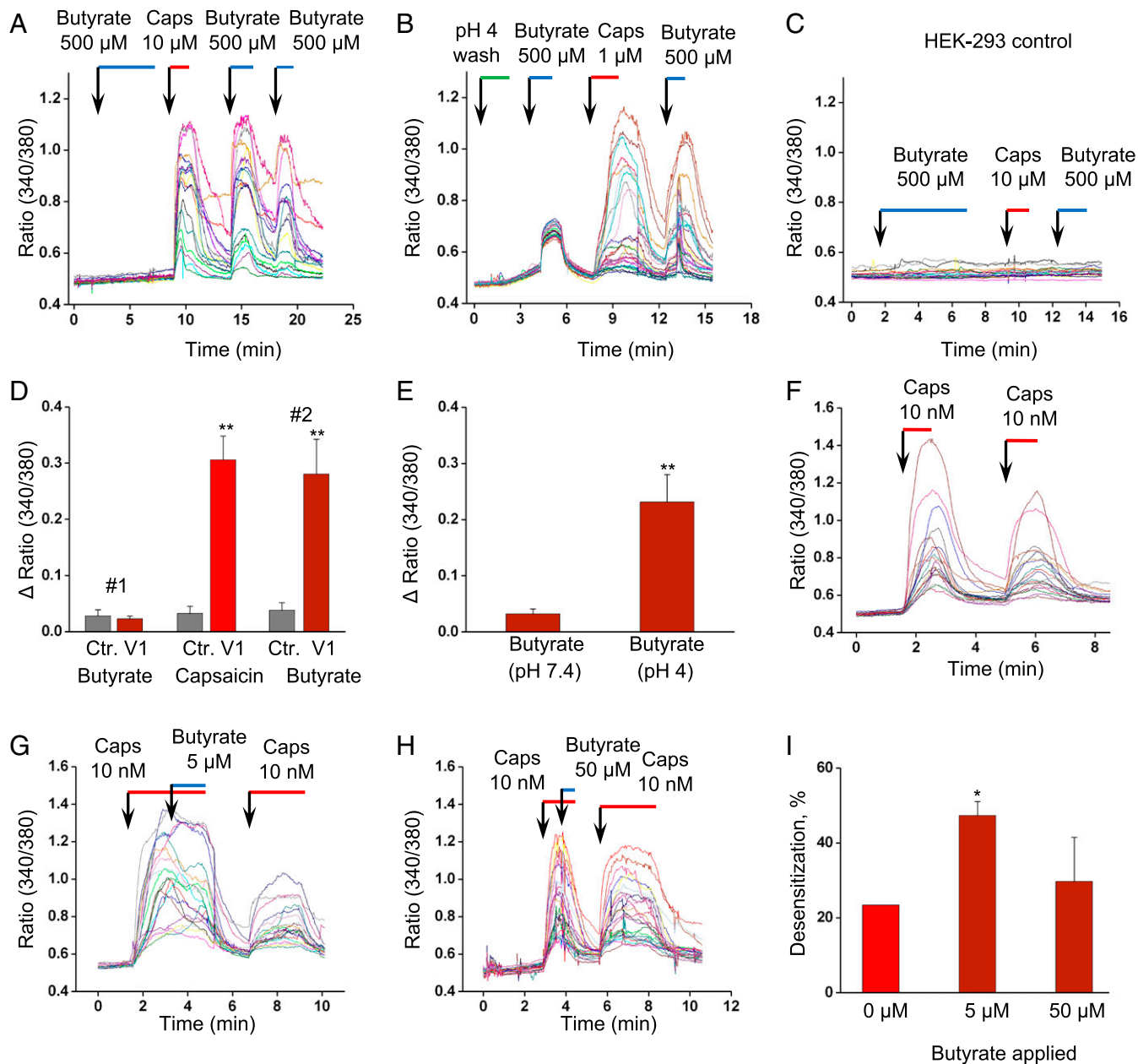
Fig. 7. Butyrate modulates TRPV1 activity as partial agonist in vitro. (*A*) 500 μM butyrate elicits TRPV1 activation after, but not prior to, capsaicin-induced channel activation. (*B*) Brief exposure to low pH conditions primes a moderate, ubiquitous TRPV1 response to 500 μM butyrate. (*C*) Control experiment. (*D*) Prior to (#1) and postcapsaicin (#2) butyrate-induced TRPV1 (labeled V1) activation ($n_{exp.} = 4$, $n_{cells} = 90$) compared to control HEK-293 cells (labeled Ctr.) ($n_{exp.} = 3$, $n_{cells} = 54$); (*E*) TRPV1 activation responses to butyrate with or without a preceding low pH buffer wash ($n_{exp.} = 6$, 5, $n_{cells} = 164$, 127); (*F*) Minimal desensitization is observed when 10 nM capsaicin is applied consecutively in the absence of butyrate. (*G*) 5 μM butyrate to TRPV1-expressing cells results in desensitization to subsequent capsaicin-induced TRPV1 activation. (*H*) 50 μM butyrate to TRPV1-expressing cells results in desensitization that tends to be lower than that seen with 5 μM. (*I*) Percent desensitization (signal of second application compared to first) is significantly greater when 5 μM butyrate is applied following the first capsaicin pulse ($n_{exp.} = 4$, $n_{cells} = 83$) compared to when butyrate is absent. Percent desensitization is intermediate when 50 μM is used ($n_{exp.} = 3$, $n_{cells} = 69$). All error bars are equal to ± SEM, *$P < 0.05$ and **$P < 0.01$.

are transported by the blood and act on peripheral tissues (34–36, 40, 57–59). Notably, differences in butyrate-metabolizing species and in serum levels of butyrate have been observed in fibromyalgia patients (31). Butyrate also improved nerve injury-associated neuropathic pain in rodents (66). Overall, these recent findings suggest that the gut microbiome is involved in nonvisceral pain. Moreover, human obesity is often accompanied by a low-grade chronic inflammation (95) and butyrate has been shown to be antiinflammatory. However, systemic inflammation is not increased after 12 to 14 wk of WD regimen (96) when

compared to 60% high fat diet (97), suggesting that, in our model, FMT may not act by preventing systemic WD-induced inflammation.

A recent report demonstrated that butyrate can facilitate M2 macrophage polarization and thus exert a therapeutic effect in a model of colitis (98). Interestingly, Ji et al. suggested that butyrate-enhanced M2 polarization could be mediated by HDAC inhibitory activity. Previous studies described butyrate as an HDAC inhibitor (25, 70). Another study indicated that HDAC2 normalization levels lead to pain alleviation following peripheral nerve injury (99). We observed an increase in *HDAC2* mRNA

Table 1. Participant characteristics (*n* = 29)

	Male (*n* = 12)	Female (*n* = 17)	*P* value
Age (y)	47.3 ± 5.2	45.4 ± 7.1	0.417
Weight (kg)	91.2 ± 29.9	95.0 ± 32.8	0.750*
BMI (kg/m^2)	29.8 ± 9.1	35.3 ± 10.7	0.168*
Obese (*n*, %)	4 (33.3)	14 (82.4)	0.013*
Diabetic (*n*, %)	1 (8.3)	3 (17.7)	0.421[†]
NQOL	4.3 ± 6.7	5.3 ± 8.2	0.741[†]
UENS	4.7 ± 5.8	6.5 ± 6.8	0.542[†]
Hypersensitive (*n*, %)	4 (33.3)	7 (41.2)	0.983[†]
Fasted blood glucose (mg/dL)	110.6 ± 59.2	117.1 ± 62.4	0.585[†]
Serum acetic acid (μM)	53.9 ± 15.7	53.0 ± 11.6	0.915[†]
Serum butyric acid (μM)	3.2 ± 0.3	2.9 ± 0.2	0.005[†]
Serum propionic acid (μM)	7.2 ± 0.6	7.1 ± 0.6	0.808[†]
Serum valeric acid (μM)	3.8 ± 0.3	3.7 ± 0.4	0.961[†]
Total serum SCFAs (μM)	68.2 ± 16.0	66.8 ± 12.2	0.868[†]

*Adjusted for age.
[†]Adjusted for age and BMI.

levels in butyrate-treated DRG organotypic culture, indicating that butyrate may alter gene transcription in DRG cells via *HDAC2*. Therefore, epigenetic changes may offer a possible mechanism through which FMT and butyrate improve indices of neuropathic pain in our model.

Our transcriptomic analyses revealed a 25-fold increase of *FFAR2* mRNA levels in the SN of WD-fed mice, suggesting that nerve cells of obese mice can respond to butyrate. The literature is currently unclear regarding the cell-specific role of FFAR2. However, recent reports have highlighted the role of FFAR2 in immune cell polarization (100, 101). Further cell-specific studies will be necessary to better delineate the role and function of FFARs in FMT-induced pain relief and in the onset of pain in obesity.

Several studies have shown that chronic neuropathic pain, including obesity-induced neuropathy, is a sensitized state in response to adaptive and maladaptive signals (102). Dietary lipids have been suggested as sensitizing molecules that lower the activation threshold of ion channels located in sensory neurons, leading to allodynia and hyperalgesia (103). TRPV1 channels have been largely studied in different models of pain, responding to different lipid signaling (104) and having a role in neuro-immune interactions in the PNS. The observed dose-dependency in TRPV1 activation revealed that physiological concentrations of butyrate desensitized TRPV1 channels in vitro and exerted a modulatory effect on channel activity. TRPV1 are heat-sensitive channels and it may appear contradictory that our data showed a positive correlation between circulating butyrate and mechanical threshold, but not between butyrate and thermal latency. It has been shown that mice lacking both TRPV1 and TRPV2 have normal thermal responses (105). Additionally, our in vitro data showed only a mild effect of butyrate on TRPV1 channel activity. Therefore, increased plasma butyrate is unlikely to completely shut down TRPV1 channel activity. Butyrate likely has multiple effects on many cell types in vivo so that the highly controlled setting in which our in vitro data were acquired can only indicate that butyrate has an effect in TRPV1 channels. Further studies are necessary to confirm the effects of butyrate on TRPV1 in in vivo models of neuropathic pain and identify any potential compensatory mechanisms. Given the pleiotropic effects of butyrate, this mechanism potentially contributes to the improvement of pain seen in WD-fed mice subjected to FMT.

In addition to DRG cells, it is important to consider that enteric projecting neurons (e.g., vagal) may be also involved in improving pain and immune cells of the nervous system, since they may directly sense local changes in gut metabolites (106, 107).

While at its early stage, the human data presented suggests a potential link between neuropathic pain and plasma SCFA levels. Our data offer insights into the pathogenesis of obesity and early diabetes-induced neuropathic pain and suggest that the gut microbiome/SCFA and their downstream pathways may represent targets to ameliorate early obesity-associated pain.

Materials and Methods

Please refer to *SI Appendix* for more details.

Animal Studies. Animal studies were conducted in accordance with recommendations in the *Guide for the Care and Use of Laboratory Animals* of the National Institutes of Health (108) and with the approval of the Loyola University Chicago Institutional Animal Care and Use Committee. Wild-type, male C57BL/6J mice (#000664) were obtained from Jackson Laboratories. The lean donor group was fed NC (Teklad LM-485), while the experimental groups were fed WD (TD88137, Teklad Diets; 42% kcal from fat, 34% sucrose by weight, and 0.2% cholesterol total; Envigo) for 14 wk, starting at 7 wk of age.

FMT. For the FMT group (treated), following antibiotic treatment, obese mice were orally gavaged with feces from lean mice daily for 2 wk. For the first 5 d of gavage, mice were fed with NC. For the sham or auto FMT groups (controls), groups were subjected to the same paradigm as the FMT group, except that mice were gavaged with either saline or with feces from obese mice (auto FMT) as indicated in corresponding figures.

Tributyrin treatment. At the end of week 12 on WD, animals were needle-fed with tributyrin (Sigma-Aldrich) or glycerol (used as vehicle) daily for 2 wk.

Bacterial DNA Isolation, 16S Quantification, and Diversity Analysis. Fecal pellets were collected and DNA extracted. qPCR was performed with universal 16S primers. The Loyola Genomic Core performed PCR of 16S rRNA V4-5 regions sequenced by the Illumina HiSeq4500 platform, as done previously (109); 16S sequences were aligned using the Silva Taxonomy Annotation, and files were uploaded to MicrobiomeAnalyst for analysis (110).

Mechanical and Thermal Sensitivities. Mechanical allodynia was assessed using calibrated Von Frey filaments (Stoelting) and thermal hyperalgesia was assessed by the Hargreaves Method (IITC Life Science) as previously described (7) and using ARRIVE (Animal Research: Reporting of In Vivo Experiments) guidelines.

Nerve Fiber Densities. Foot pads were collected from hind paws and fixed in Zamboni solution for 4 to 6 h on ice. Samples were processed for immunohistochemistry as described in detail elsewhere (111). Nerve fibers were identified by immunostaining with anti-PGP9.5 antibody (#7863-0504, AbD Serotec).

RNA Isolation, cDNA Library Construction, and Illumina Sequencing. Total RNA was extracted from the DRG and SN of mice using the RNAeasy isolation kit (Qiagen). The Northwestern Genomic Core (NuSeq) performed experiments and biostatistical analyses. Briefly full-length cDNA synthesis and amplification were carried out with the Clontech SMART-Seq v4 Ultra Low Input RNA Kit. Subsequently, Illumina sequencing libraries were prepared from the amplified full-length cDNA with the Nextera XT DNA Library Preparation Kit. The sequencing of the libraries was conducted on an Illumina NextSEq 500

Table 2. Partial correlation coefficients (*P* value) between circulating SCFAs and distal pain (NQOL) and UENS adjusted for age and sex

Partial correlation coefficient*	Distal pain (NQOL)	UENS
Butyrate (μM/kg·bw)	−0.292 (0.140)	−125 (0.533)
Propionate (μM/kg·bw)	−0.273 (0.168)	−0.083 (0.681)
Acetate (μM/kg·bw)	−0.259 (0.192)	−0.179 (0.372)
Valerate (μM/kg·bw)	−0.337 (0.085)	−0.093 (0.644)
Total SCFA (μM/kg·bw)	−0.271 (0.171)	−0.170 (0.396)

bw, body weight.
*Adjusted for age and sex.

Table 3. Linear regression model for circulating SCFAs and pain, adjusted for age and sex

Linear regression*	Beta coefficient ± SE	*P* value
Distal pain		
Butyrate (μM/kg·bw)	−12.53 ± 8.23	0.140
Propionate (μM/kg·bw)	−4.91 ± 0.15	0.168
Acetate (μM/kg·bw)	−0.43 ± 0.320	0.192
Valerate (μM/kg·bw)	−11.25 ± 6.28	0.085
Total SCFA (μM/kg·bw)	−0.390 ± 0.28	0.171
UENS		
Butyrate (μM/kg·bw)	−67.88 ± 107.47	0.533
Propionate (μM/kg·bw)	−18.80 ± 45.12	0.681
Acetate (μM/kg·bw)	−3.73 ± 4.13	0.372
Valerate (μM/kg·bw)	−39.11 ± 83.65	0.644
Total SCFA (μM/kg·bw)	−3.09 ± 3.6	0.396

*Linear regression adjusted for age and sex.

NGS System. Single 75-bp reads were generated with dual indexing. RNA sequencing analysis was done with STAR and DESeq2. The quality of reads, in FASTQ format, was evaluated using FastQC. Metascape (http://metascape.org) was used to identify enriched pathways among genes with significant differential expression (q-value < 0.05).

Neuron Dissociation and Calcium Studies. Neuron dissociation was performed as previously described (7). L4-L6 DRG were collected from NC-, WD-, and WD-fed FMT mice, axotomized, and then transferred to a collagenase A/trypsin mix (1.25 mg/mL each; Sigma Aldrich) in advanced DMEM (Corning) and incubated for 30 min at 37 °C in a 5% CO_2. Dissociated neurons were resuspended in advanced DMEM (1 g/L glucose) supplemented with 10% fetal bovine serum (FBS) (Gibco–Life Technologies) and 4 mM Gluta-MAX (Gibco–Life Technologies). An overnight serum depletion was performed before each experiment (using 2% serum, 1% BSA). At day 4, DRG neurons plated on coverslips were used for measurements of [Ca]i changes. Changes in cytosolic free Ca^{2+} concentration ($[Ca^{2+}]_i$) were measured with a laser-scanning confocal microscope (Radiance 2000 MP, Bio-Rad, and LSM 410, Zeiss) equipped with a 40× oil-immersion objective lens (N.A., 1.3). To record $[Ca^{2+}]_i$, we used the high-affinity Ca^{2+} indicator Fluo-4 (Molecular Probes/Invitrogen).

Flow Cytometry. DRG and SN dissociated cells were stained with fluorescently conjugated antibodies. Flow cytometry data were acquired using a BD FACS Aria III and data analyzed using FlowJo (Treestar).

Plasma SCFA. For mice, after decapitation under anesthesia, blood was collected in K3EDTA tubes (Sarstedt), and centrifuged at $2,000 × g$ for 10 min. For humans, blood was collected after overnight fasting and plasma was separated. The LC/MS analysis was performed on AB Sciex Qtrap 5500 coupled to Agilent UPLC/HPLC system. All of the samples were analyzed by the University of Illinois at Chicago Mass Spectrometry Core in triplicate and an internal control was used to evaluate interassay variability.

TRPV1 Studies.
Intracellular Ca^{2+} measurements. A TRPV1-transfected HEK-293 stable cell line was developed with TRPV1 tagged with *myc* on the N terminus, as previously described (112). The extracellular solution used in ratiometric $[Ca^{2+}]_i$ measurements contained: 137 mM NaCl, 5 mM KCl, 2 mM $CaCl_2$, 1 mM $MgCl_2$, 10 mM glucose, and 10 mM HEPES, pH 7.4. For low pH experiments, this buffer was adjusted to pH 3.0 or 4.0. Cells were incubated with 2 μM Fura-2 acetoxymethyl ester (Invitrogen). The measurements were performed using a Photon Technology International imaging system mounted on Zeiss-AXIO Observed D1 microscope.

Human Neuropathy Assessment. The Institutional Review Board of Loyola University Chicago (LU 209537) approved the experiments. Informed consent was obtained from all participants. A description of the participant inclusion has been previously detailed (77).
UENS examination and questionnaires. The UENS requires a number 2 (13/4 inch) safety pin and a 128-Hz tuning fork. The dorsal surface of the foot and leg was pricked by the pin, working centripetally from the great toe, in 1- to 2-cm increments, while asking the subject to respond when he/she first feels sharpness of any kind. On each side, two points were scored for each region in which the patient fails to feel any sharpness. One additional point was scored for each additional region in which the pin feels less sharp than expected [as detailed in Singleton et al. (113)]. Questionnaires in UENS evaluated evoked distal pain and sensory loss.
NeuroQol questionnaire. The unweighted NeuroQol questionnaire was used to assess physical symptoms (questions 1 to 13). Patients with results equal or higher than 3 were qualified as exhibiting distal pain (114).

Statistical Analysis. All data are represented as mean ± SEM. Analyses were performed using Origin 2018, OriginLab, and Graphpad Prism.

Data Availability. All study data are included in the article and supporting information.

1. A. Stokes et al., The contribution of obesity to prescription opioid use in the United States. *Pain* **160**, 2255–2262 (2019).
2. A. Stokes et al., The contribution of obesity to prescription opioid use in the United States. *Pain* **160**, 2255–2262, 10.1097/j.pain.0000000000001612 (2019).
3. J. C. Arezzo, E. Zotova, Electrophysiologic measures of diabetic neuropathy: Mechanism and meaning. *Int. Rev. Neurobiol.* **50**, 229–255 (2002).
4. S. Hong, T. J. Morrow, P. E. Paulson, L. L. Isom, J. W. Wiley, Early painful diabetic neuropathy is associated with differential changes in tetrodotoxin-sensitive and -resistant sodium channels in dorsal root ganglion neurons in the rat. *J. Biol. Chem.* **279**, 29341–29350 (2004).
5. C. J. Sumner, S. Sheth, J. W. Griffin, D. R. Cornblath, M. Polydefkis, The spectrum of neuropathy in diabetes and impaired glucose tolerance. *Neurology* **60**, 108–111 (2003).
6. P. D. O'Brien, L. M. Hinder, B. C. Callaghan, E. L. Feldman, Neurological consequences of obesity. *Lancet Neurol.* **16**, 465–477 (2017).
7. C. K. Gavini et al., Liver X receptors protect dorsal root ganglia from obesity-induced endoplasmic reticulum stress and mechanical allodynia. *Cell Rep.* **25**, 271–277.e4 (2018).
8. G. Aubert, V. Mansuy, M. J. Voirol, L. Pellerin, F. P. Pralong, The anorexigenic effects of metformin involve increases in hypothalamic leptin receptor expression. *Metabolism* **60**, 327–334 (2011).
9. B. L. Guilford, J. M. Ryals, D. E. Wright, Phenotypic changes in diabetic neuropathy induced by a high-fat diet in diabetic C57BL/6 mice. *Exp. Diabetes Res.* **2011**, 848307 (2011).
10. G. J. Biessels et al., Phenotyping animal models of diabetic neuropathy: A consensus statement of the diabetic neuropathy study group of the EASD (Neurodiab). *J. Peripher. Nerv. Syst.* **19**, 77–87 (2014).
11. Y. Suzuki, J. Sato, M. Kawanishi, K. Mizumura, Lowered response threshold and increased responsiveness to mechanical stimulation of cutaneous nociceptive fibers in streptozotocin-diabetic rat skin in vitro—Correlates of mechanical allodynia and hyperalgesia observed in the early stage of diabetes. *Neurosci. Res.* **43**, 171–178 (2002).
12. D. M. Menichella et al., CXCR4 chemokine receptor signaling mediates pain in diabetic neuropathy. *Mol. Pain* **10**, 42 (2014).
13. N. D. Jayaraj et al., Reducing CXCR4-mediated nociceptor hyperexcitability reverses painful diabetic neuropathy. *J. Clin. Invest.* **128**, 2205–2225 (2018).
14. T. D. Wiggin et al., Elevated triglycerides correlate with progression of diabetic neuropathy. *Diabetes* **58**, 1634–1640 (2009).
15. J. Hur et al., Transcriptional networks of murine diabetic peripheral neuropathy and nephropathy: Common and distinct gene expression patterns. *Diabetologia* **59**, 1297–1306 (2016).
16. M. Pande et al., Transcriptional profiling of diabetic neuropathy in the BKS db/db mouse: A model of type 2 diabetes. *Diabetes* **60**, 1981–1989 (2011).
17. O. A. Tashani, R. Astita, D. Sharp, M. I. Johnson, Body mass index and distribution of body fat can influence sensory detection and pain sensitivity. *Eur. J. Pain* **21**, 1186–1196 (2017).
18. E. D. Hu et al., High fiber dietary and sodium butyrate attenuate experimental autoimmune hepatitis through regulation of immune regulatory cells and intestinal barrier. *Cell. Immunol.* **328**, 24–32 (2018).
19. X. Chen, J. Xu, Y. Su, W. Zhu, Effects of intravenous infusion with sodium butyrate on colonic microbiota, intestinal development- and mucosal immune-related gene expression in normal growing pigs. *Front. Microbiol.* **9**, 1652 (2018).
20. L. Tian et al., Sodium butyrate improved intestinal immune function associated with NF-κB and p38MAPK signalling pathways in young grass carp (Ctenopharyngodon idella). *Fish Shellfish Immunol.* **66**, 548–563 (2017).
21. A. Sikandar et al., Effect of sodium butyrate on performance, immune status, microarchitecture of small intestinal mucosa and lymphoid organs in broiler chickens. *Asian-Australas. J. Anim. Sci.* **30**, 690–699 (2017).

PHYSIOLOGY

22. A. Schwarz, A. Bruhs, T. Schwarz, The short-chain fatty acid sodium butyrate functions as a regulator of the skin immune system. *J. Invest. Dermatol.* **137**, 855–864 (2017).

23. W. Liu *et al.*, Effects of dietary microencapsulated sodium butyrate on growth, intestinal mucosal morphology, immune response and adhesive bacteria in juvenile common carp (Cyprinus carpio) pre-fed with or without oxidised oil. *Br. J. Nutr.* **112**, 15–29 (2014).

24. Y. Furusawa *et al.*, Commensal microbe-derived butyrate induces the differentiation of colonic regulatory T cells. *Nature* **504**, 446–450 (2013).

25. N. Arpaia *et al.*, Metabolites produced by commensal bacteria promote peripheral regulatory T-cell generation. *Nature* **504**, 451–455 (2013).

26. J. Zhang *et al.*, Beneficial effect of butyrate-producing Lachnospiraceae on stress-induced visceral hypersensitivity in rats. *J. Gastroenterol. Hepatol.* **34**, 1368–1376 (2019).

27. X. Long *et al.*, Butyrate promotes visceral hypersensitivity in an IBS-like model via enteric glial cell-derived nerve growth factor. *Neurogastroenterol. Motil.* **30**, e13227 (2018).

28. S. A. Vanhoutvin *et al.*, The effects of butyrate enemas on visceral perception in healthy volunteers. *Neurogastroenterol. Motil.* **21**, 952-e76 (2009).

29. S. M. O' Mahony, T. G. Dinan, J. F. Cryan, The gut microbiota as a key regulator of visceral pain. *Pain* **158** (suppl. 1), S19–S28 (2017).

30. S. Shen *et al.*, Gut microbiota is critical for the induction of chemotherapy-induced pain. *Nat. Neurosci.* **20**, 1213–1216 (2017).

31. A. Minerbi *et al.*, Altered microbiome composition in individuals with fibromyalgia. *Pain* **160**, 2589–2602 (2019).

32. T. T. Cai *et al.*, Fecal microbiota transplantation relieve painful diabetic neuropathy: A case report. *Medicine (Baltimore)* **97**, e13543 (2018).

33. C. E. McMurran *et al.*, The microbiota regulates murine inflammatory responses to toxin-induced CNS demyelination but has minimal impact on remyelination. *Proc. Natl. Acad. Sci. U.S.A.* **116**, 25311–25321 (2019).

34. G. J. Bakker, J. Zhao, H. Herrema, M. Nieuwdorp, Gut microbiota and energy expenditure in health and obesity. *J. Clin. Gastroenterol.* **49** (suppl. 1), S13–S19 (2015).

35. N. C. de Clercq, M. N. Frissen, A. K. Groen, M. Nieuwdorp, Gut microbiota and the gut-brain axis: New insights in the pathophysiology of metabolic syndrome. *Psychosom. Med.* **79**, 874–879 (2017).

36. N. C. de Clercq, A. K. Groen, J. A. Romijn, M. Nieuwdorp, Gut microbiota in obesity and undernutrition. *Adv. Nutr.* **7**, 1080–1089 (2016).

37. D. J. Cabral *et al.*, Microbial metabolism modulates antibiotic susceptibility within the murine gut microbiome. *Cell Metab.* **30**, 800–823.e7 (2019).

38. H. Wang *et al.*, Promising treatment for type 2 diabetes: Fecal microbiota transplantation reverses insulin resistance and impaired islets. *Front. Cell. Infect. Microbiol.* **9**, 455 (2020).

39. P. P. Zhang *et al.*, Fecal microbiota transplantation improves metabolism and gut microbiome composition in db/db mice. *Acta Pharmacol. Sin.* **41**, 678–685 (2020).

40. K. E. Bouter, D. H. van Raalte, A. K. Groen, M. Nieuwdorp, Role of the gut microbiome in the pathogenesis of obesity and obesity-related metabolic dysfunction. *Gastroenterology* **152**, 1671–1678 (2017).

41. E. Niederberger, E. Resch, M. J. Parnham, G. Geisslinger, Drugging the pain epigenome. *Nat. Rev. Neurol.* **13**, 434–447 (2017).

42. P. Fernyhough, N. A. Calcutt, Abnormal calcium homeostasis in peripheral neuropathies. *Cell Calcium* **47**, 130–139 (2010).

43. S. E. Murthy *et al.*, The mechanosensitive ion channel Piezo2 mediates sensitivity to mechanical pain in mice. *Sci. Transl. Med.* **10**, eaat9897 (2018).

44. X. Wang *et al.*, Cytokine-like 1 chemoattracts monocytes/macrophages via CCR2. *J. Immunol.* **196**, 4090–4099 (2016).

45. H. C. Moon, Y. S. Park, Reduced GABAergic neuronal activity in zona incerta causes neuropathic pain in a rat sciatic nerve chronic constriction injury model. *J. Pain Res.* **10**, 1125–1134 (2017).

46. M. Simonetti *et al.*, Wnt-Fzd signaling sensitizes peripheral sensory neurons via distinct noncanonical pathways. *Neuron* **83**, 104–121 (2014).

47. T. L. Follansbee *et al.*, *Drosophila* nociceptive sensitization requires BMP signaling via the canonical SMAD pathway. *J. Neurosci.* **37**, 8524–8533 (2017).

48. Y. Zhang *et al.*, Peripheral pain is enhanced by insulin-like growth factor 1 through a G protein-mediated stimulation of T-type calcium channels. *Sci. Signal.* **7**, ra94 (2014).

49. A. Alunno *et al.*, Insulin-like growth factor binding protein 6 in rheumatoid arthritis: A possible novel chemotactic factor? *Front. Immunol.* **8**, 554 (2017).

50. N. A. Calcutt *et al.*, Selective antagonism of muscarinic receptors is neuroprotective in peripheral neuropathy. *J. Clin. Invest.* **127**, 608–622 (2017).

51. F. A. Pinho-Ribeiro, W. A. Verri Jr., I. M. Chiu, Nociceptor sensory neuron-immune interactions in pain and inflammation. *Trends Immunol.* **38**, 5–19 (2017).

52. S. D. Brain, T. J. Williams, Inflammatory oedema induced by synergism between calcitonin gene-related peptide (CGRP) and mediators of increased vascular permeability. *Br. J. Pharmacol.* **86**, 855–860 (1985).

53. U. Andersson, K. J. Tracey, Reflex principles of immunological homeostasis. *Annu. Rev. Immunol.* **30**, 313–335 (2012).

54. R. R. Ji, A. Chamessian, Y. Q. Zhang, Pain regulation by non-neuronal cells and inflammation. *Science* **354**, 572–577 (2016).

55. K. K. Beiswenger, N. A. Calcutt, A. P. Mizisin, Epidermal nerve fiber quantification in the assessment of diabetic neuropathy. *Acta Histochem.* **110**, 351–362 (2008).

56. J. Schulthess *et al.*, The short chain fatty acid butyrate imprints an antimicrobial program in macrophages. *Immunity* **50**, 432–445.e7 (2019).

57. H. Herrema, R. G. IJzerman, M. Nieuwdorp, Emerging role of intestinal microbiota and microbial metabolites in metabolic control. *Diabetologia* **60**, 613–617 (2017).

58. D. Samocha-Bonet *et al.*, Metabolically healthy and unhealthy obese—The 2013 Stock Conference report. *Obes. Rev.* **15**, 697–708 (2014).

59. M. Nieuwdorp, P. W. Gilijamse, N. Pai, L. M. Kaplan, Role of the microbiome in energy regulation and metabolism. *Gastroenterology* **146**, 1525–1533 (2014).

60. A. Wichmann *et al.*, Microbial modulation of energy availability in the colon regulates intestinal transit. *Cell Host Microbe* **14**, 582–590 (2013).

61. M. Müller *et al.*, Circulating but not faecal short-chain fatty acids are related to insulin sensitivity, lipolysis and GLP-1 concentrations in humans. *Sci. Rep.* **9**, 12515 (2019).

62. X. Zou *et al.*, Effects of sodium butyrate on intestinal health and gut microbiota composition during intestinal inflammation progression in broilers. *Poult. Sci.* **98**, 4449–4456 (2019).

63. Q. Zhang *et al.*, Accelerated dysbiosis of gut microbiota during aggravation of DSS-induced colitis by a butyrate-producing bacterium. *Sci. Rep.* **6**, 27572 (2016).

64. F. Rivera-Chávez *et al.*, Depletion of butyrate-producing clostridia from the gut microbiota drives an aerobic luminal expansion of Salmonella. *Cell Host Microbe* **19**, 443–454 (2016).

65. R. Hodin, Maintaining gut homeostasis: The butyrate-NF-kappaB connection. *Gastroenterology* **118**, 798–801 (2000).

66. A. Kukkar, N. Singh, A. S. Jaggi, Attenuation of neuropathic pain by sodium butyrate in an experimental model of chronic constriction injury in rats. *J. Formos. Med. Assoc.* **113**, 921–928 (2014).

67. R. Corrêa-Oliveira, J. L. Fachi, A. Vieira, F. T. Sato, M. A. Vinolo, Regulation of immune cell function by short-chain fatty acids. *Clin. Transl. Immunol.* **5**, e73 (2016).

68. C. H. Kim, Immune regulation by microbiome metabolites. *Immunology* **154**, 220–229 (2018).

69. B. Dalile, L. Van Oudenhove, B. Vervliet, K. Verbeke, The role of short-chain fatty acids in microbiota-gut-brain communication. *Nat. Rev. Gastroenterol. Hepatol.* **16**, 461–478 (2019).

70. J. R. Davie, Inhibition of histone deacetylase activity by butyrate. *J. Nutr.* **133** (suppl. 7), 2485S–2493S (2003).

71. M. J. Caterina *et al.*, The capsaicin receptor: A heat-activated ion channel in the pain pathway. *Nature* **389**, 816–824 (1997).

72. Y. Nersesyan *et al.*, Oxytocin modulates nociception as an agonist of pain-sensing TRPV1. *Cell Rep.* **21**, 1681–1691 (2017).

73. H. Lin, Y. An, F. Hao, Y. Wang, H. Tang, Correlations of fecal metabonomic and microbiomic changes induced by high-fat diet in the pre-obesity state. *Sci. Rep.* **6**, 21618 (2016).

74. K. S. Fluitman, M. Wijdeveld, M. Nieuwdorp, R. G. IJzerman, Potential of butyrate to influence food intake in mice and men. *Gut* **67**, 1203–1204 (2018).

75. K. Bouter *et al.*, Differential metabolic effects of oral butyrate treatment in lean versus metabolic syndrome subjects. *Clin. Transl. Gastroenterol.* **9**, 155 (2018).

76. G. Navarro *et al.*, Gut microbial features can predict host phenotype response to protein deficiency. *Physiol. Rep.* **6**, e13932 (2018).

77. L. R. Dugas *et al.*, Gut microbiota, short chain fatty acids, and obesity across the epidemiologic transition: The METS-Microbiome study protocol. *BMC Public Health* **18**, 978 (2018).

78. L. R. Dugas *et al.*, Decreased microbial co-occurrence network stability and SCFA receptor level correlates with obesity in African-origin women. *Sci. Rep.* **8**, 17135 (2018).

79. F. Wang *et al.*, Morphine induces changes in the gut microbiome and metabolome in a morphine dependence model. *Sci. Rep.* **8**, 3596 (2018).

80. A. G. Smith *et al.*, Lifestyle intervention for pre-diabetic neuropathy. *Diabetes Care* **29**, 1294–1299 (2006).

81. G. L. Pittenger *et al.*, Intraepidermal nerve fibers are indicators of small-fiber neuropathy in both diabetic and nondiabetic patients. *Diabetes Care* **27**, 1974–1979 (2004).

82. J. Boyette-Davis, P. M. Dougherty, Protection against oxaliplatin-induced mechanical hyperalgesia and intraepidermal nerve fiber loss by minocycline. *Exp. Neurol.* **229**, 353–357 (2011).

83. P. Anand *et al.*, Rational treatment of chemotherapy-induced peripheral neuropathy with capsaicin 8% patch: From pain relief towards disease modification. *J. Pain Res.* **12**, 2039–2052 (2019).

84. D. Morales *et al.*, Association between peripheral neuropathy and exposure to oral fluoroquinolone or amoxicillin-clavulanate therapy. *JAMA Neurol.* **76**, 827–833 (2019).

85. L. Z. Cheng, N. Lü, N. Y. Q. Zhang, Z. Q. Zhao, Ryanodine receptors contribute to the induction of nociceptive input-evoked long-term potentiation in the rat spinal cord slice. *Mol. Pain* **6**, 1 (2010).

86. M. D. Sanna, D. Peroni, A. Quattrone, C. Ghelardini, N. Galeotti, Spinal RyR2 pathway regulated by the RNA-binding protein HuD induces pain hypersensitivity in antiretroviral neuropathy. *Exp. Neurol.* **267**, 53–63 (2015).

87. D. Shakiryanova *et al.*, Presynaptic ryanodine receptor-activated calmodulin kinase II increases vesicle mobility and potentiates neuropeptide release. *J. Neurosci.* **27**, 7799–7806 (2007).

88. J. M. McNally *et al.*, Functional ryanodine receptors in the membranes of neurohypophysial secretory granules. *J. Gen. Physiol.* **143**, 693–702 (2014).

89. B. Inceoglu *et al.*, Endoplasmic reticulum stress in the peripheral nervous system is a significant driver of neuropathic pain. *Proc. Natl. Acad. Sci. U.S.A.* **112**, 9082–9087 (2015).

90. B. Entaz, K. Hyongsuk, Y. Hyonok, ER stress-mediated signaling: Action potential and Ca2+ as key players. *Int. J. Mol. Sci.* **17**, 1558 (2016).

91. E. J. Cobos *et al.*, Mechanistic differences in neuropathic pain modalities revealed by correlating behavior with global expression profiling. *Cell Rep.* **22**, 1301–1312 (2018).

92. P. Italiani, D. Boraschi, From monocytes to M1/M2 macrophages: Phenotypical vs. functional differentiation. *Front. Immunol.* **5**, 514 (2014).

93. X. Yu *et al.*, Dorsal root ganglion macrophages contribute to both the initiation and persistence of neuropathic pain. *Nat. Commun.* **11**, 264 (2020).

94. W. Feng, H. Ao, C. Peng, Gut microbiota, short-chain fatty acids, and herbal medicines. *Front. Pharmacol.* **9**, 1354 (2018).

95. R. Monteiro, I. Azevedo, Chronic inflammation in obesity and the metabolic syndrome. *Mediators Inflamm.* **2010**, 289645 (2010).

96. M.-A. Virginie *et al.*, Loss of the liver X receptor LXRα/β in peripheral sensory neurons modifies energy expenditure. *eLife* **4**, e06667 (2015).

97. V. Mansuy-Aubert *et al.*, Imbalance between neutrophil elastase and its inhibitor α1-antitrypsin in obesity alters insulin sensitivity, inflammation, and energy expenditure. *Cell Metab.* **17**, 534–548 (2013).

98. J. Ji *et al.*, Microbial metabolite butyrate facilitates M2 macrophage polarization and function. *Sci. Rep.* **6**, 24838 (2016).

99. B. Ouyang *et al.*, Normalizing HDAC2 levels in the spinal cord alleviates thermal and mechanical hyperalgesia after peripheral nerve injury and promotes GAD65 and KCC2 expression. *Front. Neurosci.* **13**, 346 (2019).

100. M. K. Nøhr *et al.*, GPR41/FFAR3 and GPR43/FFAR2 as cosensors for short-chain fatty acids in enteroendocrine cells vs FFAR3 in enteric neurons and FFAR2 in enteric leukocytes. *Endocrinology* **154**, 3552–3564 (2013).

101. M. K. Nøhr *et al.*, Expression of the short chain fatty acid receptor GPR41/FFAR3 in autonomic and somatic sensory ganglia. *Neuroscience* **290**, 126–137 (2015).

102. R. Kuner, H. Flor, Structural plasticity and reorganisation in chronic pain. *Nat. Rev. Neurosci.* **18**, 113 (2017).

103. T. Osthues, M. Sisignano, Oxidized lipids in persistent pain states. *Front. Pharmacol.* **10**, 1147 (2019).

104. V. Lukacs, J. M. Rives, X. Sun, E. Zakharian, T. Rohacs, Promiscuous activation of transient receptor potential vanilloid 1 (TRPV1) channels by negatively charged intracellular lipids: The key role of endogenous phosphoinositides in maintaining channel activity. *J. Biol. Chem.* **288**, 35003–35013 (2013).

105. C. J. Woodbury *et al.*, Nociceptors lacking TRPV1 and TRPV2 have normal heat responses. *J. Neurosci.* **24**, 6410–6415 (2004).

106. N. Y. Lai *et al.*, Gut-innervating nociceptor neurons regulate Peyer's patch microfold cells and SFB levels to mediate Salmonella host defense. *Cell* **180**, 33–49.e22 (2020).

107. A. Dance, Inner workings: How bacteria cause pain and what that reveals about the role of the nervous system. *Proc. Natl. Acad. Sci. U.S.A.* **116**, 12584–12586 (2019).

108. National Research Council, *Guide for the Care and Use of Laboratory Animals*, (National Academies Press, Washington, DC, 8th Ed., 2011).

109. M. M. Pearce *et al.*, The female urinary microbiome: A comparison of women with and without urgency urinary incontinence. *MBio* **5**, e01283-14 (2014).

110. J. Chong, P. Liu, G. Zhou, J. Xia, Using MicrobiomeAnalyst for comprehensive statistical, functional, and meta-analysis of microbiome data. *Nat. Protoc.* **15**, 799–821 (2020).

111. C. G. Jolivalt *et al.*, Peripheral neuropathy in mouse models of diabetes. *Curr. Protoc. Mouse Biol.* **6**, 223–255 (2016).

112. E. Zakharian, B. Thyagarajan, R. J. French, E. Pavlov, T. Rohacs, Inorganic polyphosphate modulates TRPM8 channels. *PLoS One* **4**, e5404 (2009).

113. J. R. Singleton *et al.*, The Utah Early Neuropathy Scale: A sensitive clinical scale for early sensory predominant neuropathy. *J. Peripher. Nerv. Syst.* **13**, 218–227 (2008).

114. L. Vileikyte *et al.*, The development and validation of a neuropathy- and foot ulcer-specific quality of life instrument. *Diabetes Care* **26**, 2549–2555 (2003).

PHYSIOLOGY